

# GSA DATA REPOSITORY 2012172

## The viscous-brittle transition of crystal bearing silicic melt: direct observation of magma rupture and healing.

B. Cordonnier<sup>1,2</sup>

L. Caricchi<sup>3</sup>

M. Pistone<sup>1</sup>

J. Castro<sup>4</sup>

K.-U. Hess<sup>5</sup>

S. Gottschaller<sup>5</sup>

M. Manga<sup>2</sup>

D.B. Dingwell<sup>5</sup>

L. Burlini<sup>1</sup>

1. Geological Institute, Swiss Federal Institute of Technology, Zurich.
2. Department of Earth and Planetary Science, University of California, Berkeley
3. Department of Earth Sciences, University of Bristol.
4. Institute of Geosciences, University of Mainz, Mainz, Germany.
5. Department of Earth and Environmental Sciences, Ludwig-Maximilians-University, Munich.

### Methods

A mixture of fine powdered oxides was melted twice at  $T=1700$  K for 6h and then quenched to a glass. The resulting glass was ground to a fine powder and mixed with different proportions of corundum particles to obtain samples characterized by different crystal fractions. These mixtures were subsequently cold pressed (40 ton load) in canisters (50 mm diameter 200 mm length hollow cylinders) made of stainless steel alloy EN 1.4301 (Kohler Zurich). The prepared powder is chemically insulated from the canister with molybdenum foil. The containers were subsequently welded and immersed in a water bath under vacuum to check for perfect closure. The samples were synthesized in a large volume internally heated pressure vessel (42 liters heated volume of argon) at 170 MPa and 1373 K for 24 hours.

The melt composition is a haplogranite melt (HPG8) with 5% mole excess sodium. The viscosity and its temperature dependence of this specific composition were experimentally measured and confirm the model of Hess et al. (1995). We ensured that no unexpected reactions occurred by re-measuring the chemical composition of the interstitial melt after each experiment (see table 1).

The samples were cooled at about 60K/min to  $T=900$ K, which corresponds to a viscosity of about  $10^{11}$  Pa·s (Hess et al., 1995) and then cooled at 0.6 K/min until room temperature was reached. This procedure ensures the relaxation of the stresses in the sample related to cooling. The average projected length of the admixed particles is 1.37 mm with a standard deviation of 0.25 mm. Their aspect ratio is slightly elongated ranging from 1 to 3 with an average of 1.4 and a standard deviation of 0.2. Thus, the suspension is similar to mono-dispersed spheres (Saar et al., 2001), which simplifies the whole system complexity. However, the outlines of the crushed corundum particles deviate from that of ideal spheres by exhibiting the irregular patterns resulting from concoidal fracturing (see Figure 1). In order to characterise the crystal fraction and its network, the resulting products were scanned with neutron tomography and directly observed in thin-sections. We checked that the glass was crack-free and had the predicted

crystal fraction (see table 2). Our samples do not contain volatiles and are consequently a pure two-phase material. Moreover, the deformation experiments were performed at higher confining pressure than the synthesis to ensure that any residual gas phase would remain dissolved in the melt.

Cylindrical samples of 15 mm diameter and 10 mm length were directly drilled from the containers used for the synthesis and double polished to obtain parallel surfaces (allowed deviation about 2 microns). The samples were placed in the centre of a symmetric assembly composed of cylinders of alumina and partially stabilized zirconia ceramic. The column was inserted in an iron tube, isolating the sample from the argon gas used as pressure confining medium. The experiments were carried out in an internally heated Paterson-type deformation apparatus (Paterson and Olgaard, 2000) at the Rock Deformation Laboratory of ETH Zurich (Switzerland). The deformation tests were performed at 200 and 300 MPa confining pressure and temperatures between 873 and 1173 K by applying simple shear stresses in a torsion configuration (Paterson and Olgaard, 2000). All the experiments were carried out by applying fixed strain-rates to the sample and performing a strain-rate stepping test, where once a constant value of stress is reached the strain-rate is increased to a higher value. (Paterson and Olgaard, 2000). The strain-rate is thus gradually increased toward the critical strain-rate (see eq. 2). While doing so, we continued to measure the stress applied to the sample and we stopped the experiment if stress instabilities were detected. This was done to prevent damage to the apparatus and to confirm that the small stress drops are in fact caused by creating cracks. Micro-cracking is manifest through stress instabilities: when cracks are initiated the stress decreases the applied stress to conserve the defined constant strain-rate. The applied stress is obtained from the torque exerted from the apparatus on the sample. The contribution of the jacket is subtracted from the total torque and the stress applied obtained from the equation

$$\tau = M \frac{4(3+n)}{\pi d^3},$$

where  $M$  is the torque [N·m],  $d$  is the diameter of the sample [m], and  $n$  is the flow index, the exponent of a power-law type fluid and the characteristic parameter of the stress/strain rate dependence. It is obtained from the relation  $d \log(M) / d \log(\dot{\theta})$  where  $\dot{\theta}$  is the twist-rate [rad·s<sup>-1</sup>], and evaluated from the stress steps performed before failure. The  $n$  exponent calculation is only valid for a continuous and homogeneous cylindrical sample. At relatively low stresses, we found exponents in agreement with those obtained by Arbaret et al. (2007) and Caricchi et al. (2007) who used similar materials. The  $n$  exponent sensitivity is, however, dependent of the number of steps performed in the low stress field. Thus experiments with only a few steps have poorly constrained values of the  $n$  exponent. Moreover while approaching failure, the flow index drops and a second flow regime is observed. This last one is consistent with the brittle behavior observed at atmospheric pressure (Cordonnier et al., 2009) and was called transition regime to emphasize the switch from viscous to brittle regime. Thus the continuity and homogeneity hypotheses may no longer be justified and the choice of the flow index ( $n$ ) is problematic. However the maximal error between a Newtonian fluid ( $n=1$ ) and a rigid-plastic material ( $n=0$ ) is a stress change of of 25%. In Figure 3, the error bars represents the difference between Newtonian fluids ( $n=1$ ) and plastic fluids ( $n=0$ ). The flow index of the 0.65 crystal fraction could not be calculated in our experiments but is estimated around 0.25 from previous work (Arbaret et al., 2007; Caricchi et al., 2007).

Nineteen experiments were performed, some with several stress steps and other by going directly to the critical stress in order to confirm that strain had little effect. The details of each experiment are reported in table 3 and plotted in Figure 2.

Table DR1: Melt Chemical composition in weight %, average of 86 counts performed in the melt phase of the sample. FeO\* is the total iron measured. StD: Standard deviation. The measurements were performed under the protocol of (Morgan and London, 1996, 2005).

	<b>Weight %</b>	<b>StD</b>
SiO <sub>2</sub>	75.73	0.57
TiO <sub>2</sub>	0.01	0.01
Al <sub>2</sub> O <sub>3</sub>	11.41	0.25
FeO*	0.01	0.01
MnO	0.01	0.01
MgO	0.01	0.01
CaO	0.01	0.02
Na <sub>2</sub> O	8.24	0.27
K <sub>2</sub> O	3.98	0.15
P <sub>2</sub> O <sub>5</sub>	0.01	0.01
<i>Total</i>	<i>99.98</i>	<i>0.61</i>

Table DR2: Results of crystal fraction estimate before deformation compared to expected values from sample preparation using weight fraction calculation. 1) Point Counting Methods, Average of 500 counts, 2) Stereo-Microscopy Method (reflected light), Average of 3500 counts. 3) Thresholding Method, Average of 7 image analysis. 4) Point Counting Method on Tomographic results of the 3D Xray- $\mu$ CT scans, Average of 7 image analysis. StD: Standard deviation. Point counting performed in random grid mode using the Software JMicroVision.

Preparation	Expected	PCM [1]	SMM [2]	StD	TM [3]	StD	PCM-T [4]
110-1	15	12.80	14.65	2.05	16.50	2.05	
140-2	40						39.44
140-3	40	40.80	41.13	2.08	42.59	2.08	
155-2	55	56.80	55.89	2.54	57.30	0.99	
265-1	65	68.20	57.83	2.54	61.23	1.40	
265-2	65						63.76
265-4	65	63.00	61.14	4.17	62.77	1.09	

Table DR3: Experimental Results.

Experiment number	Crystal Fraction [%]	Confining Pressure [MPa]	Temperature [C]	Strain-rate [s <sup>-1</sup> ]	Strain	Cumulated strain	Peak of stress (n=1) [Pa]	Peak of stress (n=.5) [Pa]	Peak of stress (n=.25) [Pa]	Peak of stress (n=infty) [Pa]	n exponent	Peak of stress used in Figures. [Pa]	Failure
Exp. #01	15	200	600.7	7.6E-04	0.897	0.897	2.94E+7	2.57E+7	2.39E+7	2.20E+7	1.00	2.94E+7	no
	15	200	601.1	8.5E-04	0.551	1.448	3.33E+7	2.92E+7	2.71E+7	2.50E+7	1.00	3.33E+7	no
Exp. #02	15	200	600.9	3.4E-04	0.091	0.091	1.44E+7	1.26E+7	1.17E+7	1.08E+7	1.00	1.44E+7	no
	15	200	600.4	3.7E-04	0.151	0.242	1.52E+7	1.33E+7	1.23E+7	1.14E+7	1.00	1.52E+7	no
	15	200	600.4	5.6E-04	0.210	0.452	2.33E+7	2.04E+7	1.90E+7	1.75E+7	1.00	2.33E+7	no
	15	200	600.6	7.5E-04	0.504	0.956	3.23E+7	2.83E+7	2.63E+7	2.42E+7	1.00	3.23E+7	no
	15	200	601.2	8.6E-04	0.331	1.287	3.59E+7	3.15E+7	2.92E+7	2.70E+7	1.00	3.59E+7	no
Exp. #03	15	200	600.9	9.5E-04	0.301	1.588	4.04E+7	3.54E+7	3.29E+7	3.03E+7	1.00	4.04E+7	no
	15	200	595.3	3.0E-03	0.780	0.780	1.08E+8	9.45E+7	8.78E+7	8.10E+7	0.68	9.94E+7	yes
Exp. #04	15	200	576.3	3.7E-03	0.370	0.374	1.15E+8	1.01E+8	9.34E+7	8.63E+7	0.44	9.89E+7	yes
Exp. #05	40	200	603.3	1.4E-04	0.342	0.342	1.98E+7	1.73E+7	1.61E+7	1.49E+7	0.87	1.91E+7	no
Exp. #06	40	200	654.2	1.3E-04	0.030	0.030	1.39E+6	1.22E+6	1.13E+6	1.04E+6	0.90	1.36E+6	no
	40	200	654.2	6.8E-04	0.221	0.252	8.58E+6	7.51E+6	6.97E+6	6.44E+6	0.90	8.36E+6	no
Exp. #07	40	200	654.2	1.0E-03	0.524	0.775	1.32E+7	1.16E+7	1.07E+7	9.90E+6	0.90	1.28E+7	no
	40	200	600.7	5.0E-05	0.062	0.062	1.92E+7	1.68E+7	1.56E+7	1.44E+7	0.87	1.85E+7	no
Exp. #08	40	200	600.6	1.0E-04	1.144	1.206	3.31E+7	2.90E+7	2.69E+7	2.48E+7	0.87	3.20E+7	no
	40	300	624.4	5.0E-05	0.066	0.066	8.92E+6	7.81E+6	7.25E+6	6.69E+6	0.68	8.20E+6	no
	40	300	624.4	1.0E-04	0.068	0.134	1.47E+7	1.29E+7	1.19E+7	1.10E+7	0.68	1.35E+7	no
	40	300	624.4	3.0E-04	0.259	0.393	3.17E+7	2.77E+7	2.58E+7	2.38E+7	0.68	2.91E+7	no
Exp. #09	40	300	624.4	7.5E-04	1.118	1.510	5.26E+7	4.60E+7	4.27E+7	3.95E+7	0.55	4.67E+7	no
	40	300	624.4	9.9E-04	0.305	1.815	5.76E+7	5.04E+7	4.68E+7	4.32E+7	0.33	4.80E+7	yes
	40	200	600.5	3.7E-05	0.043	0.043	7.88E+6	6.90E+6	6.40E+6	5.91E+6	0.87	7.63E+6	no
	40	200	600.5	2.2E-03	0.396	0.439	5.73E+7	5.01E+7	4.66E+7	4.30E+7	0.49	5.00E+7	yes
Exp. #10	55	300	734.5	6.4E-05	0.043	0.043	4.90E+6	4.29E+6	3.98E+6	3.68E+6	0.92	4.80E+6	no
	55	300	734.6	1.1E-04	0.114	0.157	9.30E+6	8.14E+6	7.56E+6	6.98E+6	0.92	9.11E+6	no
	55	300	734.6	5.0E-04	0.406	0.563	1.95E+7	1.71E+7	1.58E+7	1.46E+7	0.60	1.76E+7	no
	55	300	734.5	1.0E-03	0.597	1.160	2.07E+7	1.81E+7	1.68E+7	1.55E+7	0.08	1.59E+7	yes
Exp. #11	55	300	704.7	1.1E-05	0.020	0.066	3.62E+6	3.17E+6	2.94E+6	2.72E+6	0.51	3.17E+6	no
	55	300	704.7	6.4E-05	0.079	0.099	9.03E+6	7.90E+6	7.34E+6	6.77E+6	0.51	7.93E+6	no
	55	300	704.7	1.1E-04	0.073	0.172	1.19E+7	1.04E+7	9.67E+6	8.93E+6	0.50	1.04E+7	no
	55	300	704.7	5.0E-04	0.535	0.707	2.44E+7	2.14E+7	1.98E+7	1.83E+7	0.50	2.13E+7	no
Exp. #12	55	300	704.7	1.0E-03	0.315	1.022	2.86E+7	2.50E+7	2.32E+7	2.15E+7	0.00	2.15E+7	yes
	55	200	750.2	1.1E-05	0.037	0.037	1.17E+7	1.02E+7	9.51E+6	8.78E+6	0.46	1.01E+7	no
	55	200	750.2	2.5E-05	0.081	0.118	1.70E+7	1.49E+7	1.38E+7	1.28E+7	0.46	1.47E+7	no
	55	200	750.2	5.0E-05	0.168	0.286	2.41E+7	2.11E+7	1.96E+7	1.81E+7	0.46	2.09E+7	no
	55	200	750.2	7.5E-05	0.224	0.509	2.81E+7	2.46E+7	2.28E+7	2.11E+7	0.42	2.40E+7	no
Exp. #13	55	200	750.2	1.0E-04	0.133	0.642	2.89E+7	2.53E+7	2.35E+7	2.17E+7	0.42	2.47E+7	no
	55	200	750.2	2.5E-04	0.090	0.732	3.04E+7	2.66E+7	2.47E+7	2.28E+7	0.05	2.32E+7	yes
	55	200	800.8	1.2E-05	0.023	0.023	1.75E+6	1.53E+6	1.42E+6	1.31E+6	0.89	1.70E+6	no
	55	200	800.8	1.2E-04	0.294	0.317	1.36E+7	1.19E+7	1.11E+7	1.02E+7	0.82	1.30E+7	no
	55	200	800.8	3.7E-04	1.289	1.605	2.64E+7	2.31E+7	2.15E+7	1.98E+7	0.61	2.38E+7	yes
Exp. #14	55	200	750.1	7.3E-05	0.016	0.016	1.05E+7	9.19E+6	8.53E+6	7.88E+6	0.34	8.78E+6	no
	55	200	750.1	5.1E-04	0.042	0.058	1.97E+7	1.72E+7	1.60E+7	1.48E+7	0.34	1.65E+7	no
	55	200	750.1	1.0E-03	0.093	0.151	2.46E+7	2.15E+7	2.00E+7	1.85E+7	0.33	2.05E+7	no
	55	200	750.1	1.5E-03	0.148	0.298	2.84E+7	2.49E+7	2.31E+7	2.13E+7	0.33	2.36E+7	no
Exp. #15	65	300	804.7	8.7E-05	0.138	0.138	3.56E+7	3.12E+7	2.89E+7	2.67E+7	0.25	2.89E+7	yes
Exp. #16	65	300	905.0	5.0E-05	0.082	0.082	1.96E+7	1.72E+7	1.59E+7	1.47E+7	0.25	1.59E+7	yes
Exp. #17	65	300	854.7	5.0E-05	0.292	0.292	3.61E+7	3.15E+7	2.93E+7	2.70E+7	0.25	2.93E+7	yes
Exp. #18	65	200	900.0	5.0E-05	0.097	0.097	3.31E+7	2.90E+7	2.69E+7	2.48E+7	0.25	2.69E+7	yes
Exp. #19	65	200	900.8	2.0E-05	0.267	0.267	4.58E+7	4.01E+7	3.72E+7	3.44E+7	0.25	3.72E+7	yes

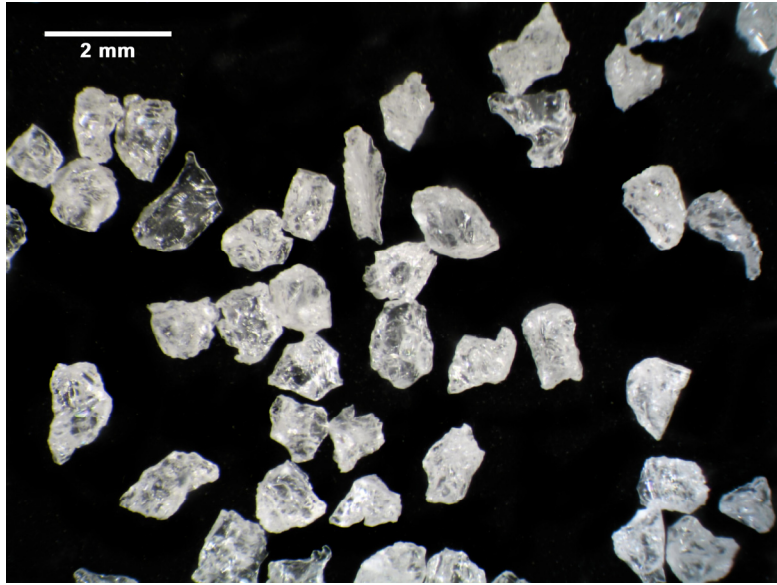


Figure DR1: Typical corundum crystals used for the synthesis of the samples.

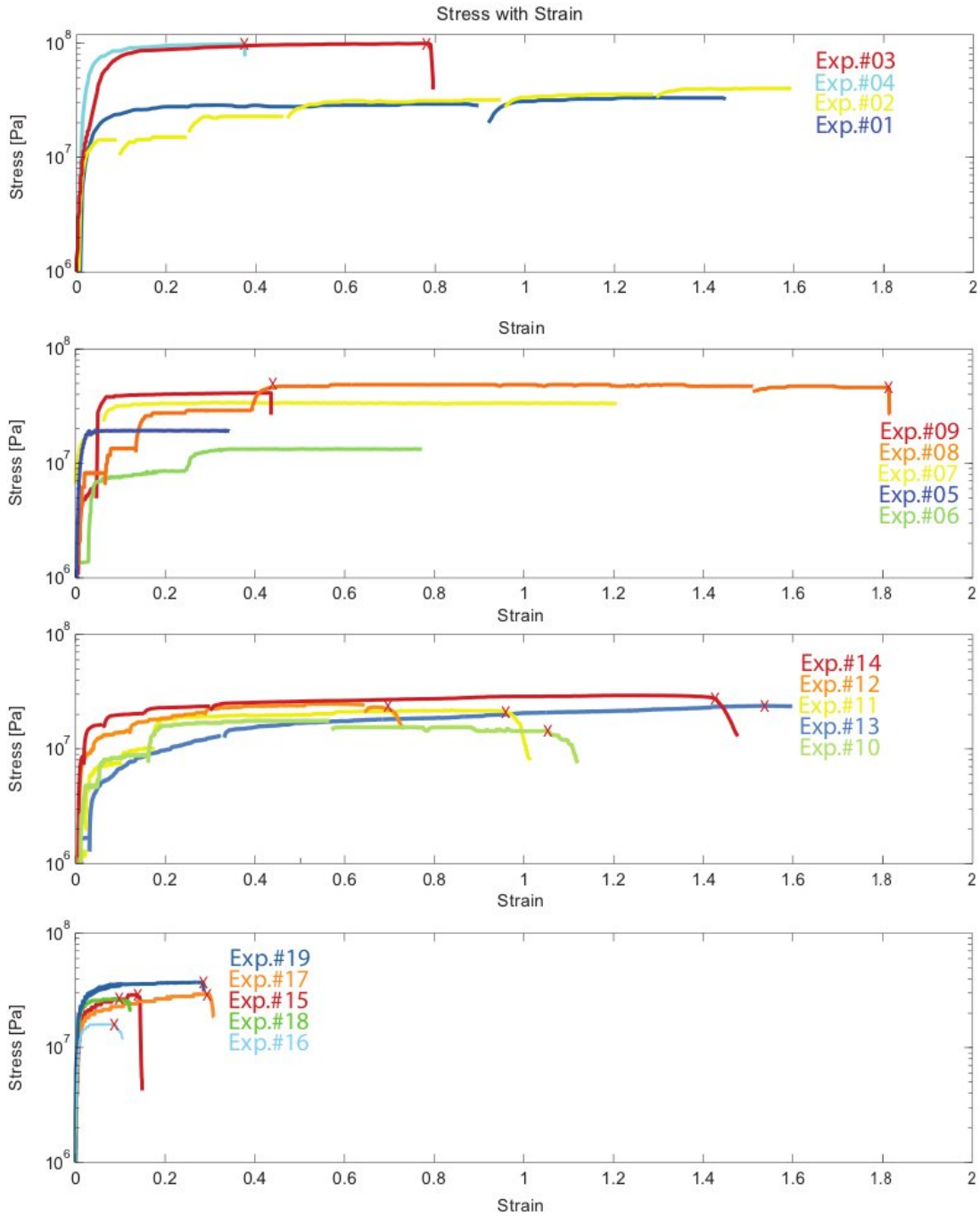


Figure DR2: Measured stress versus accumulated strain for all the experiments detailed in table 3. Crosses indicate the failure of the sample.

## References

- Arbaret, L., Bystricky, M., and Champallier, R., 2007, Microstructures and rheology of hydrous synthetic magmatic suspensions deformed in torsion at high pressure: *Journal of Geophysical Research-Solid Earth*, v. 112, p. 24.
- Caricchi, L., Burlini, L., Ulmer, P., Gerya, T., Vassalli, M., and Papale, P., 2007, Non-Newtonian rheology of crystal-bearing magmas and implications for magma ascent dynamics: *Earth and Planetary Science Letters*, v. 264, p. 402-419.
- Cordonnier, B., Hess, K.U., Lavallee, Y., and Dingwell, D.B., 2009, Rheological properties of dome lavas: Case study of Unzen volcano: *Earth and Planetary Science Letters*, v. 279, p. 263-272.
- Hess, K.U., Dingwell, D.B., and Webb, S.L., 1995, The Influence of Excess Alkalis on the Viscosity of a Haplogranitic Melt: *American Mineralogist*, v. 80, p. 297-304.
- Morgan, G.B., VI, and London, D., 1996, Optimizing the electron microprobe analysis of hydrous alkali aluminosilicate glasses: *American Mineralogist*, v. 81, p. 1176-1185.
- , 2005, Effect of current density on the electron microprobe analysis of alkali aluminosilicate glasses: *American Mineralogist*, v. 90, p. 1131-1138.
- Paterson, M.S., and Olgaard, D.L., 2000, Rock deformation tests to large shear strains in torsion: *Journal of Structural Geology*, v. 22, p. 1341-1358.
- Saar, M.O., Manga, M., Cashman, K.V., and Fremouw, S., 2001, Numerical models of the onset of yield strength in crystal-melt suspensions: *Earth and Planetary Science Letters*, v. 187, p. 367-379.